

Modelling Battery-free Communications for the Cooja Simulator

Carlos Pérez-Penichet, Georgios Theodoros Daglaridis, Dilushi Piumwardane, Thiemo Voigt*

Uppsala University, Sweden. *Uppsala University and RISE SICS, Sweden.
carlos.penichet@it.uu.se, george.daglaridis@it.uu.se, dilushi.piumwardane@it.uu.se, thiemo@sics.se

Abstract

Recent progress on backscatter communications enable devices that, assisted by an unmodulated carrier, receive and transmit standard wireless protocols such as IEEE 802.15.4 with sub-milliwatt power consumption. This paradigm, that we call carrier-assisted communications, enables battery-free devices due to its reduced power consumption. To develop at scale, and integrate seamlessly into networks of unmodified conventional nodes, we need novel protocols at the MAC layer and above that can coordinate the carrier generators with receivers and transmitters while maintaining energy and spectral efficiency. A highly effective tool to develop such protocols is a network simulator. We introduce models for the communication range, energy consumption and other characteristics of carrier-assisted links based on parameters gathered from real-world experiments. We implement the models in Cooja, a well-known simulator, creating the first carrier-assisted communications framework to simulate interoperable battery-free devices alongside conventional sensor nodes. We illustrate how such a tool can offer valuable insights in the development and evaluation of efficient protocols for carrier-assisted communications.

Categories and Subject Descriptors

C.2 [Computer-Communication Networks]: Networks Architecture and Design

General Terms

Battery-free communications

Keywords

Backscatter, Battery-free, Simulation model, Cooja

1 Introduction

Battery-free devices that operate only on energy harvested from their environment are attractive for novel applications that range from wearables [14] and medical im-

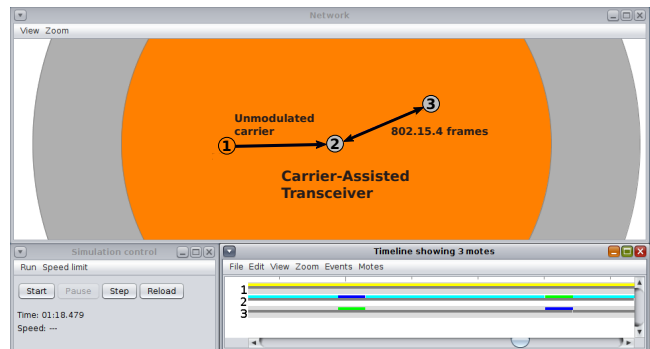


Figure 1. Our Cooja extension simulates carrier-assisted communications. Node 1, a conventional IEEE 802.15.4 node, generates an unmodulated carrier so that the carrier-assisted transceiver (Node 2) can send and receive 802.15.4 frames from Node 3, also a conventional node.

plants [34] to localization [20, 22] and smart cities [32]. While communications has traditionally been a major hurdle for these applications, the situation is changing due to a new class of carrier-assisted communication devices with dramatically reduced power consumption. These devices can transmit and receive standard wireless protocols such as IEEE 802.15.4 [6, 7, 14, 15, 24, 25] while assisted by an external carrier. The key advantage is that they enable battery-free devices that could seamlessly integrate with existing standard sensor networks. One could envision extending the sensing capabilities of an existing network without adding new batteries and creating an explosion of maintenance costs [24]. To add new sensing capabilities, one simply adds a battery-free device that contains the sensor. The device transmits its readings using carrier-assisted communications to a nearby conventional node with the assistance of a second conventional node which uses its radio test mode [24] to provide the necessary unmodulated carrier.

The next step in realizing this integration is the development of novel communication protocols above the physical layer tailored to this new class of devices. Communicating with these devices has the added complexity of the need for the unmodulated carrier. Hence, the most important objective for these protocols will be coordinating between carrier generator, transmitter and receiver, preserving energy efficiency and reducing collisions caused by the carrier.

In this paper we introduce realistic models to simulate carrier-assisted communications, in particular for receivers with an external Local Oscillator (LO) [6, 25] that are not modelled by existing works. We extend Cooja [21], a well-known network simulator, to enable, for the first time, simulations of carrier-assisted devices alongside conventional nodes (Figure 1). We focus on the communications aspect of these devices and not on other issues such as energy harvesting. We argue that a tool like this will be instrumental in the development of this new kind of carrier-assisted communication protocols at the MAC layer and above.

Contribution. We introduce models to simulate radio links for carrier-assisted transceivers, the combination of a backscatter transmitter and a carrier-assisted receiver (Figure 4), in a realistic but simple manner. Our models accurately reproduce a variety of effects, such as multiple backscatter reflections, that stem from the way these new devices operate and that could have significant impact in the development of future communication protocols for these devices. Although our models are general, we implement them in Cooja to simulate heterogeneous networks of standard-compatible carrier-assisted IEEE 802.15.4 devices that operate alongside unmodified conventional sensor nodes (Figure 1). In a network like this, the conventional nodes already implemented in Cooja can play the roles of transmitter, receiver and carrier generator in communications to and from the carrier-assisted ones. Our implementation extends existing Cooja functionality to carrier-assisted communications enabling the evaluation and comparison of the energy consumption of battery-free protocols through simulation. The extended Cooja is available for the community to use from: <https://github.com/cperezpenichet/contiki-ng/tree/carrier-assisted>

We make the following specific contributions:

- Simple but realistic models for carrier-assisted communications, extracting key parameters from experimental results and ensuring the model captures special characteristics of carrier-assisted links. This enables realistic simulations of carrier-assisted communications.
- We integrate carrier-assisted devices in Cooja, maintaining compatibility with existing devices and mechanisms. This enables, for example, energy estimation to help develop and evaluate communication protocols for battery-free devices.
- We show how such a tool can offer key insights to develop future communication protocols for the integration of battery-free devices into standard IoT networks.

Challenges. Frameworks such as Castalia [5] and Cooja simulate radio links by modelling them in a simplified way that still captures the most relevant electromagnetic (EM) phenomena for communications. Carrier-assisted radio links differ qualitatively from traditional ones in key aspects such as range and vulnerability to interference. This is because the behavior of carrier-assisted radio links depends on the strength of the external unmodulated carrier. There is no general model in the literature for carrier-assisted communications. While there are works on simulating backscatter communications [10, 19, 35], they focus on standard RFID

tags and readers that employ RFID-specific protocols. By contrast, our goal is to simulate a new kind of tags that interoperate directly (without a dedicated reader) with unmodified IoT devices using standard IoT protocols such as IEEE 802.15.4. These new tags are possible thanks to new techniques such as frequency-shifted backscatter and reception with an external LO that are not modelled by previous works.

The way these devices operate leads to unprecedented effects in traditional radio links. For example, to prevent creating interference with the unmodulated carrier at the receiver, carrier-assisted devices have a mechanism to shift their transmissions in frequency. These mechanisms, however, could also reflect other transmissions creating frequency-shifted interference in undesired ways. Because of the potential impact of these effects in the development and evaluation of future communication protocols, it is imperative that they are accurately reproduced by the simulator.

Approach. We introduce a carrier-assisted radio link model based on a combination of theoretical results from the literature and from our own experiments. The experimental results allow us to model the signal reception at the carrier-assisted device and to obtain realistic values for key parameters. We take great care to ensure that our simulator is able to reproduce the most significant particular effects, such as frequency-shifted interference or multiple backscatter reflections given the potential impact of these phenomena in future protocols for these devices. Finally, we validate our model against experimental results to verify its accuracy making sure that it reproduces those effects faithfully.

Results. Our models can accurately simulate carrier-assisted communication links in a way that is consistent with experimental results. Our simulations capture important effects such as multiple backscatter reflections and frequency-shifted interference. We believe this could be instrumental in the design of future communication protocols for battery-free devices that employ carrier-assisted communication techniques.

Furthermore, we show that our implementation of carrier-assisted communications in Cooja is compatible with the existing energy estimation methods within the platform. This is a fundamental feature for the evaluation and comparison of future protocols for severely energy-constrained devices. To illustrate this, we simulate several MAC protocols and compare their energy efficiency using our Cooja extension.

To the best of our knowledge this is the first simulation solution for standard-compatible carrier-assisted communications. Our tool enables advancing the integration of carrier-assisted devices with unmodified standard IoT nodes.

Outline. We continue our paper with some necessary background in Section 2. In Section 3 we present our extensions to the Cooja simulator. Section 4 contains an evaluation of our implementation while Section 5 presents related work. We conclude our work in Section 6.

2 Background

In this section we introduce the necessary background to model carrier-assisted communications. We begin with an introduction to carrier-assisted communications, pointing out important differences to conventional radios. We then

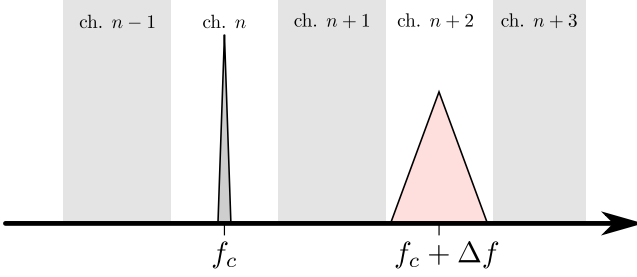


Figure 2. Frequency-shifted backscatter spectrum. The backscattered signal is reflected at a frequency $f_c + \Delta f$, two channels above the unmodulated carrier (frequency f_c), to avoid self-interference from the carrier at the receiver.

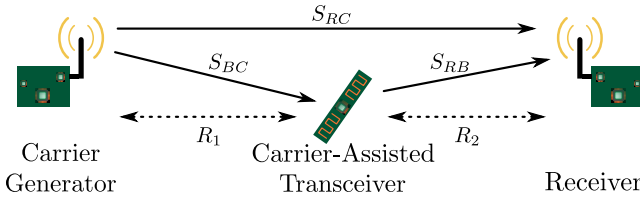


Figure 3. Signals involved in a backscatter radio link. There is potential for self-interference from the unmodulated carrier (S_{RC}) at the receiver.

discuss the basic characteristics of this type of radio links.

2.1 Carrier-assisted Communications

Carrier-assisted transceivers leverage an external unmodulated carrier both for transmissions and for reception. To transmit, the device employs backscatter communications while for reception it employs a receiver with an external carrier in place of a local oscillator. We now present the operating principles of each of the two techniques.

802.15.4 backscatter transmissions. Backscatter transmitters work by reflecting an external Radio Frequency (RF) signal in a way that conveys useful information [15, 18]. This technique is attractive because it lowers the power consumption of traditional radios by up to three orders of magnitude. The transmitter toggles a switch that selects the load attached to its antenna, purposely creating an impedance mismatch that controls the way the incident RF is reflected. A receiver can observe the changes in the reflected signal to decode the transmitted information. Because the phase changes of the reflected signal can be controlled this way, a backscatter transmitter can transmit Offset-Quadrature Phase Shift Keying (O-QPSK) as required by the IEEE 802.15.4 standard [13]. The standard also defines the channel assignment used by compatible devices, it specifies 16 channels spaced every 5 MHz in the 2.4 GHz ISM band. Backscatter transmissions of 802.15.4 compatible signals have been demonstrated in previous works [15, 24].

Frequency-shifted backscatter. One important technique that enables backscattering standard commodity wireless protocols is that the signal can be reflected at a different frequency than the necessary unmodulated carrier. This allows the receiver to avoid interference from the strong unmodulated carrier while still receiving the weak backscattered signal by placing the latter at a different channel than the for-

mer (Figure 2). The signal observed at the receiver (S_{RX}) is the superposition of the one coming from the backscatter device and the one coming directly from the carrier generator (Figure 3). Namely: $S_{RX} = S_{RC} + S_{RB}$.

S_{RB} is proportional to the product of the signal reaching the backscatter antenna (S_{BC}) and the signal driving the switch ($B(t)$), which is the complex baseband signal [14, 18].

$$S_{RX} = S_{RC} + \beta B(t)S_{BC} \quad (1)$$

Where β is the complex attenuation coefficient for the backscattered signal. Considering the case of an unmodulated carrier of frequency f_c and a complex sinusoid of frequency Δf emulated by periodically switching among complex impedances [14], the product $B(t)S_{BC}$ results in

$$2e^{j2\pi\Delta f t} \cos(2\pi f_c t) = e^{j2\pi(f_c + \Delta f)t} + e^{j2\pi(-f_c + \Delta f)t}.$$

This shows how the product results a single frequency-shifted image of frequency $f_c + \Delta f$ (Figure 2), as the second term has negative frequency and does not appear in practice. One can leverage this property to avoid interference from the unmodulated carrier at the receiver, since the baseband signal is shifted away from the carrier frequency [14, 33]. We have earlier shown that, for IEEE 802.15.4, placing the backscattered signal 10 MHz (two channels) away from the unmodulated carrier practically eliminates all interference from the carrier at the receiver [24].

An important consequence of frequency-shifted backscatter is that it will shift any signal impinging on the device's antenna, even if the signals are in different frequencies. This creates the potential for inadvertently reflecting interference into undesired channels if, for instance, there is an active transmitter operating nearby while a backscatter transmission is happening. At the same time, multiple concurrent unmodulated carriers will create multiple reflected signals at the corresponding frequencies [31].

Carrier-assisted 802.15.4 receiver. In a way analogous to backscatter, an external carrier can help a receiver operate with a power consumption well under 1 mW [6, 25]. Such a carrier-assisted receiver sidesteps power-hungry blocks commonly found in traditional radio receivers such as local oscillators and Analog-to-Digital Converters (ADCs) by employing passive circuits whenever possible. Specifically it offloads the LO to an external device that broadcasts an unmodulated carrier 10 MHz (two channels) below the frequency of the received signal. The receiver then employs a passive diode mixer to downconvert the RF signal to a low Intermediate Frequency (IF), where it can be further treated easily and efficiently. We have previously demonstrated a receiver that applies this technique to receive 802.15.4 signals with sub-milliwatt power consumption [25].

An important consequence of a receiver design like this is that it is more vulnerable to interference than its conventional counterparts. Because this receiver uses a single diode mixer and only the most basic input filters [6, 25], it is vulnerable to image frequencies of the diode mixer [23]. As a consequence, any pair of signals that is two channels or less apart from each other will create interference for the receiver.

A receiver of this kind, when paired with a 802.15.4 backscatter transmitter enables battery-free devices that directly interoperate with unmodified 802.15.4 transceivers while assisted by an external carrier. This significantly lowers the bar for applications where battery-free devices interoperate with standard wireless sensor nodes operating as transmitters, receivers and carrier generators. Employing the radio test mode present in commercial 802.15.4 transceivers allows those devices to fulfil the role of carrier generator, which avoids the need for any additional infrastructure to integrate battery-free devices into existing networks [24, 31]. We design our Cooja extension to simulate such scenarios and their impact on the efficiency of higher-layer protocols.

2.2 Carrier-assisted Link Characterization

Carrier-assisted radio links have particular characteristics that differ significantly from traditional ones. In both kinds of links, the information carrying signal is emitted from one device and received at another after suffering a certain path loss. In carrier-assisted links, however, the carrier must additionally be supplied through a radio link from an external device. The need for an external carrier is the main difference between carrier-assisted communication devices and their traditional counterparts.

Signal strength for backscatter transmissions. The Radar Range equation [2, 15] describes the power (P_r) of a backscattered signal observed at a receiver and coming from a backscatterer device separated from the carrier generator by a distance R_1 and from the receiver by a distance R_2 (Figure 3).

$$P_r = \left(\frac{\lambda^2 P_t G_t}{16\pi^2 R_1^2} \right) \left(G_b^2 \alpha \frac{|\Delta\Gamma|^2}{4} \right) \left(\frac{\lambda^2 G_r}{16\pi^2 R_2^2} \right) \quad (2)$$

Here P_t is the output power of the unmodulated carrier, G_t , G_b and G_r are the antenna gains of the carrier generator, battery-free device and receiver respectively, λ is the wavelength of the signal, α is a constant that describes losses incurred in modulating the signal using backscatter and $|\Delta\Gamma|^2$ is the backscatter coefficient [15], which is a measure of the efficiency of the backscatter process.

Equation 2 describes a signal strength that increases as the battery-free device approaches either the receiver or the carrier generator but it is minimized in the central point between the two (see theoretical curve in Figure 7). This is in contrast to traditional radio links which are stronger close to the transmitter and then decrease in strength as the receiver moves away.

Communication range in backscatter transmissions. At a high level we can consider that a signal needs to surpass the sensitivity threshold of the receiver for it to be decoded. Equation 2 forces a behavior of the signal strength that results in two areas where the signal strength could overcome the sensitivity threshold of a receiver. The first such area is next to the carrier generator and the second one is next to the receiver [15]. This is also in contrast with traditional radio links where there is a single zone of flawless reception surrounding the transmitter.

Carrier-assisted receiver sensitivity. The sensitivity of carrier-assisted receivers depends on the strength of the un-

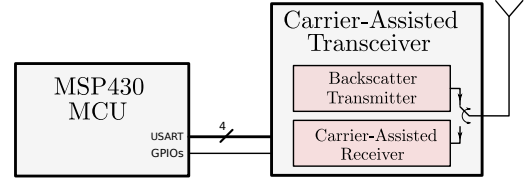


Figure 4. Battery-free device model. We model the battery-free device as a TI MSP430 MCU connected to a carrier-assisted transceiver via USART port. The carrier assisted transceiver consists of a backscatter transmitter and a carrier-assisted receiver.

modulated carrier signal [25]. Carrier-assisted receivers rely on a passive diode mixer to downconvert the RF signal at sufficiently low power consumption. The efficiency of the diode mixer (conversion loss [23]), depends on the strength of the unmodulated carrier [25]. This is the main reason why, unlike in traditional receivers, there is no single sensitivity value in these devices. Instead, we must model the dependency of the sensitivity on the incident unmodulated carrier signal strength.

Communication range in carrier-assisted receivers. The dependency of the sensitivity of the receiver upon the carrier signal strength is mirrored on the communication range. This leads to a situation where, similar to backscatter transmitters, there are two zones where the receiver operates flawlessly: When it is placed in the vicinity of the carrier generator and when it is close to the transmitter. As a result, carrier-assisted receivers exhibit a behavior analogous to the two zones of error-free communication that are observed in backscatter transmitters [25].

3 Simulator Design

We describe details of the models for carrier-assisted communications along with their implementation Cooja. We begin with a description of the battery-free device model, then introduce the radio models and finally describe energy estimation for carrier-assisted communications.

3.1 Battery-free Device Model

Our battery-free device model (Figure 4) consists of a TI MSP430 MCU connected via USART to a carrier-assisted transceiver model inspired by our previous work [25]. The carrier-assisted transceiver employs a backscatter transmitter to send information and a carrier-assisted receiver to receive data. We add a new mote type in Cooja that is analogous to other platforms that are Cooja already implemented but with the traditional radio replaced by a carrier-assisted transceiver. For instance, the Tmote Sky platform consists of a TI MSP430 MCU paired with a TI CC2420 802.15.4 transceiver IC and several additional peripherals.

During operation, the MCU can exchange data and commands via USART with the transceiver in order to send and receive data, as well as to control and configure the device. One can employ the Contiki operating system to program the device and leverage many of the tools that Contiki provides such as the network stack and energy estimation facilities that we leverage in our work. Cooja can run binaries from other operating systems such as TinyOS [16] provided that a driver for our battery-free device is written.

3.2 Radio Model

In this section we discuss the modeling and implementation details of the new Cooja extension necessary to support carrier-assisted communications.

Cooja models the probability of successful reception as a function of the signal strength at the receiver. The radio medium model decides if a given frame is received based on the signal strength, the sensitivity threshold and other factors such as interference. As discussed in Section 2, in the case of carrier-assisted communications, the probability of reception depends on the strength of the unmodulated carrier. This dependency has different root causes for backscatter transmissions and for carrier-assisted reception (i.e., Radar Range equation and diode mixer conversion loss respectively). Hence, we model them separately in different ways. We now describe how we model each of these cases in our extended Cooja implementation and then we discuss the radio medium model that ties everything together.

Modeling backscatter transmissions. The strength of a backscattered signal can be computed with the Radar Range equation (Equation 2) as discussed in Section 2. We use Equation 2 to compute the power of the signal that arrives at any receiver in range of a transmitting backscatterer device. Every parameter in Equation 2 is known except for R_1 and R_2 , the distance to the carrier generator and the receiver respectively, and $|\Delta\Gamma|^2$ the backscatter coefficient. The distances R_1 and R_2 are obtained from the simulation engine at runtime at the beginning of each transmission. The backscatter coefficient is a constant that characterizes each backscatterer device. To offer a realistic default value for $|\Delta\Gamma|^2$ we extract it from a set of experimental measurements.

We arrange a set of nodes as in Figure 3. A TmoteSky mote acts as a carrier generator at a distance $R_1 = 25$ cm apart from the carrier-assisted transceiver prototype. We then place three different TmoteSky receiver nodes at roughly two meters from the prototype ($R_2 \approx 200$ cm). This experiment is performed inside an anechoic chamber to discard the effects of multipath propagation and interference. The carrier generator transmits on channel 19 ($\lambda \approx 12.2$ cm) while the receiver is tuned to channel 21 ($\Delta f = 10$ MHz). We sweep the output power of the carrier generator (P_t) over its whole range from -25 dBm to 0 dBm. For every carrier output power, the receiver nodes measure the received signal strength (RSSI) for 30 seconds while the prototype constantly shifts the carrier by $\Delta f = 10$ MHz into the receivers' channel. This allows the receivers to measure the signal strength on the reception channel (P_r) for every carrier output power. Each of the signal strength values, represents a measurement point of Equation 2 with different combinations of values for P_t and P_r but everything else equal. From this set of measurements, we solve Equation 2 for the only remaining unknown which is $|\Delta\Gamma|^2$. Since we have many different measurements at different points of the Radar Range equation curve, but all with the same expected value of $|\Delta\Gamma|^2$, we can average them to reduce uncertainty.

Figure 5 shows a CDF of the values obtained for $|\Delta\Gamma|^2$. The result is based on 13941 individual Received Signal Strength Indicator (RSSI) samples obtained with varying values of the carrier output power. We adopt the mean value

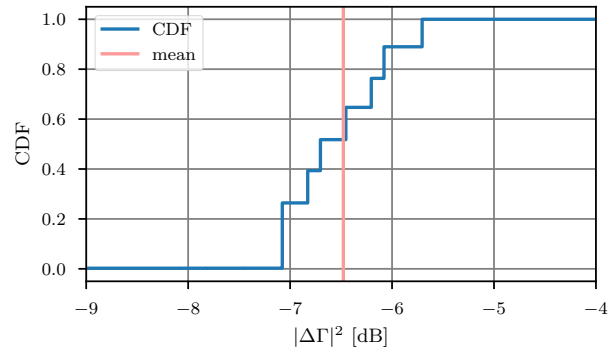


Figure 5. Cumulative distribution of the backscatter coefficient ($|\Delta\Gamma|^2$). The distribution was obtained from 13941 RSSI samples for different carrier output powers. The mean value of $|\Delta\Gamma|^2$ is -6.5 dB.

as the value of the backscatter coefficient in our simulations: $|\Delta\Gamma|^2 = -6.5$ dB. Even though there is a certain spread in the values obtained they are all within ± 1 dB of the mean value which is very good.

Modeling carrier-assisted reception. In order for the radio medium to determine if the carrier-assisted receiver should receive any given frame, it will compare the received signal strength with the sensitivity threshold of the receiver. As discussed in Section 2, the sensitivity of the carrier-assisted receiver depends on the strength of the carrier signal. We model this from experimental results gathered from a carrier-assisted receiver prototype. We measure the sensitivity of the receiver through a range of carrier signal input powers and empirically extract the dependency of the sensitivity with the carrier signal strength.

To measure the sensitivity we setup an experiment with three devices: A conventional 802.15.4 node operating as a transmitter, a carrier generator and the receiver prototype. The three devices are wired together using an RF divider combiner to avoid any external noise and multipath propagation. An Ettus B200 Software Defined Radio (SDR) acts as the carrier generator, since it allows for greater flexibility and precision in performing power sweeps. For every value of the carrier signal strength, the transmitter output power is swept. For every combination of carrier and transmitter output power, we send a long series packets with a 20 byte-long PPDU while the prototype records all received packets. We measure the Packet Reception Ratio (PRR) in each instance and from this data we compute the sensitivity for every carrier output power. We adopt the definition of sensitivity dictated by the IEEE 802.15.4 standard [13]: The threshold received signal strength where the PRR drops below 99% for a 20-byte PPDU.

Figure 6 shows the observed dependency of the sensitivity of the prototype versus carrier signal strength. The results show that the receiver is more sensitive the stronger the carrier signal is. That is, for stronger carrier signals, the receiver is able to receive weaker 802.15.4 signals. Conversely, for weaker carriers, a stronger data-carrying signal is needed to overcome the sensitivity threshold.

To obtain a generalized model of the dependency of the

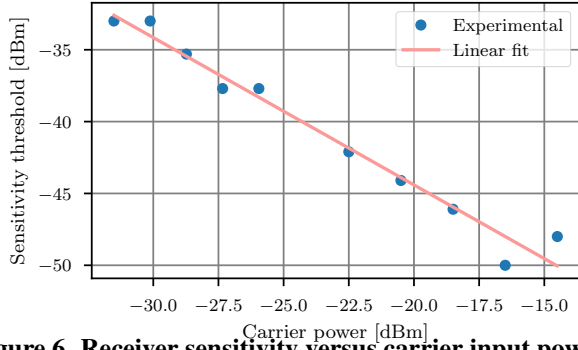


Figure 6. Receiver sensitivity versus carrier input power. We model the receiver sensitivity in Cooja with the following empirical law obtained from the experimental data via linear regression: $P_{thr} = -P_{cg} - 65$ dBm.

sensitivity threshold of the receiver with the carrier signal strength, we perform a least squares regression of the experimental data of Figure 6. Performing a simple linear fit yields a coefficient of determination $R^2 = 0.97$, indicating that the linear model is more than enough to reproduce our experimental data. We model the carrier-assisted receiver’s sensitivity threshold (P_{thr}) in Cooja with the following equation:

$$P_{thr} = A \times P_{cg} + B \quad (3)$$

Were P_{cg} is the carrier signal strength at the carrier-assisted device, $A = -1$ and $B = -65$ dBm.

Design of radio medium in Cooja. In the Cooja simulator, the radio medium is a component that simulates RF propagation. This is the component that determines if frames can be decoded at a receiver or not based on rules established by a model. These rules are responsible for simulating effects such as path loss, communication range and interference. Cooja comes with several such models to account for the characteristics of diverse environments. To model carrier-assisted communications, we introduce a new model that we call “Unit Disk Graph Medium for Carrier-Assisted Communications (UDGMCA) with Distance Loss”. Our model, like the traditional unit disk medium, is based on uniform free-space propagation and defines a circular area of flawless reception with a hard cut-off at the edge. Unlike the regular unit disk model, the UDGMCA model employs inverse square law propagation via the Radar Range equation (Equation 2) and the Friis equation [2] to dynamically compute parameters that depend on the carrier signal strength. This model is appropriate for carrier-assisted communications because they are unlikely to experience effects such as multipath propagation due to their short range. We experimentally observe the hard cutoff in measurements such as the ones in Figures 8 and 9.

The UDGMCA model defines two circular regions with different radii centered at the backscatter transmitter. The smaller disc represents the communication range and the larger disc represents the area of potential interference in case multiple transmissions overlap. The size of these discs depends on the carrier signal strength, which varies with the distance to the carrier generator. Thus, their radii have to

be determined dynamically during simulation. The radio medium utilizes Equation 2 to determine them. As long as the received signal strength is above the sensitivity threshold of the receiver, and no other signal reaches it on the same channel, then the frame can be received. If the signal strength is below the sensitivity of the receiver by 3 dB or less, the transmission cannot be received but it can still interfere transmissions reaching the same receiver. Weaker signals are ignored.

When a carrier-assisted device starts a backscatter transmission, the radio medium will check for one or more incident carriers across all channels. For every incident carrier, the medium will compute the corresponding communication and interference ranges using Equation 2. The medium then checks for any receiver within the communication range that is also listening in the shifter channel (two channels above by default) of the corresponding carrier (due to frequency-shifted backscatter). Any receiver that is found is notified of the start of the transmission and will be subsequently notified of the transmitted data. Additionally, any ongoing transmission that is detected within the interference range and the proper channel will be interfered by the new backscatter transmission. Finally, due to frequency-shifted backscatter, any transmission (modulated or not) that is in range of the backscatter device will be reflected into the corresponding reflected channel, potentially interfering with communications there.

We now discuss the way the radio medium models packet reception for carrier-assisted devices. When a transmission is starting with a carrier-assisted receiver in range, the radio medium will check if the receiver is already receiving a single unmodulated carrier and that it is in the appropriate channel. If these conditions are not met, reception fails. If the single-carrier condition is met, the medium will compute the sensitivity threshold corresponding to the carrier signal strength using Equation 3 as described before. The UDGMCA medium then compares the received signal strength to the sensitivity threshold. If the signal is above the threshold, it will be received but if it is up to 3 dB below the threshold, the receiver will be considered interfered. Otherwise, the transmission will be ignored.

The values of parameters such as $|\Delta\Gamma|^2$ and Δf are user-configurable to support any future device.

3.3 Energy Estimation

There are three different mechanisms available in Cooja for energy estimation: First, Powertracker is a Cooja native method to measure the average simulated radio duty cycle. Second, Energest is an energy estimation mechanism built into Contiki OS that can also be simulated in Cooja. Finally, Powertrace is Contiki’s energy profiling mechanism based on Energest. Because low power consumption is essential in the design of future protocols for battery-free devices, we have implemented all three mechanisms to work with the carrier-assisted transceiver. We now give a brief overview of how these three mechanisms work and how they are implemented for our carrier-assisted extension.

Powertracker. The operation of Powertracker is based on Cooja observing the percentage of simulated time that the

radio device spends in the Idle, Reception or Transmission states. From these values Cooja computes the average radio duty cycle. Our carrier-assisted transceiver model naturally supports these three states, so it inherently supports Powertracker. Powertracker is moderately useful in that it can only provide an average of the radio duty cycle. Other mechanisms are more useful in helping estimate the actual energy consumption of the radio device.

Energest. The Contiki operating system includes Energest in order to accurately estimate the energy consumption of IoT nodes. Energest is a module that tracks the time the radio spends in each of the states: Idle, Transmission and Reception. Energest is normally notified of state changes by the Contiki radio driver. We have implemented a custom Contiki radio driver for carrier-assisted transceivers to be able to use this mechanism in our extended Cooja simulator. The driver takes care of notifying the Energest module of any state changes so that it can track the energy consumption. Because the new driver conforms to the standard Contiki radio driver interface, it allows the carrier-assisted transceiver to seamlessly integrate into the Contiki protocol stack without any further changes. The driver works equally well for simulations within Cooja as with a real hardware prototype.

Powertrace. The Powertrace module leverages Energest to provide a summarized power profile of the device at specific points during execution. Once Energest is implemented for the carrier-assisted driver, Powertrace is also supported.

4 Evaluation

We take three steps to evaluate our radio model and Cooja extension. We first compare simulated results to real world experiments to show that they are in agreement within the UDGMCAs capabilities. We then show how our model properly reproduces a series of phenomena that are specific to carrier-assisted devices, such as frequency-shifted interference. Finally, we illustrate how the new simulation features can be useful in developing and evaluating communication protocols for carrier-assisted devices with a MAC protocol development scenario.

4.1 Simulation of Basic Functionality

The most basic functionality of the carrier-assisted transceiver is the ability to transmit and receive 802.15.4 frames. To demonstrate how this ability is modelled and simulated in Cooja, we reproduce a series of experiments in the simulation environment and compare the results to their real-world equivalents.

The goal of our first experiment is to reproduce in simulation the received signal strength and communication range of a backscatter transmitter as described in Section 2.

Setup. We place two conventional 802.15.4 nodes as in Figure 3, separated by a distance $R_1 + R_2$. One of the nodes emits an unmodulated carrier on channel 18 at 0 dBm while the other one works as receiver on channel 20 to account for frequency-shifted backscatter. We also place a carrier-assisted device at different positions along the line joining the conventional nodes, so as to vary the value of R_1 while keeping $R_1 + R_2$ constant. At each position, we measure the PRR and the strength of the signal backscattered by the carrier-assisted device as observed by the receiver. All three

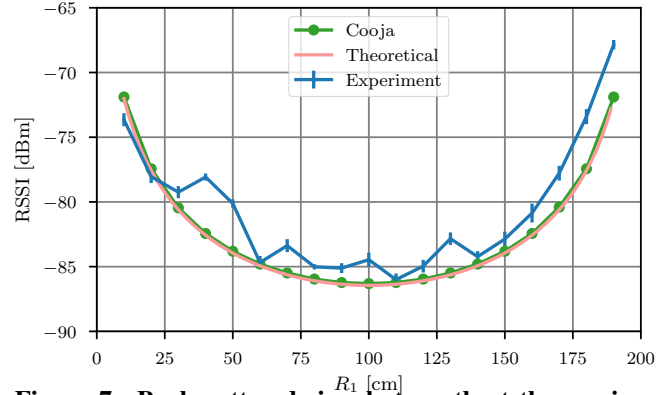


Figure 7. Backscattered signal strength at the receiver for $R_1 + R_2 = 200$ cm. The theoretical curve and the Cooja simulation are in close agreement with the experimental results.

devices have 3 dBi antennas. This experiment is performed in an anechoic chamber to avoid the effects of interference and multipath propagation. The same experiment is then simulated in Cooja for comparison.

Result. Figure 7 shows a comparison between the signal strength at the receiver as theoretically predicted by the Radar Range equation (Equation 2), as experimentally observed and as simulated in Cooja for $R_1 + R_2 = 200$ cm. The theoretical curve and the Cooja simulation closely match the experiment, showing that the expected behavior is reproduced in by our model in Cooja. Note that the discrepancies with the experimental curve are reasonably small and are likely due to experimental error or small RF effects unaccounted for by Equation 2.

Figure 8 shows a comparison of the experimental PRR result and the simulated one for $R_1 + R_2 = 300$ cm. In this case there is also a close agreement between both results. Specifically, we correctly reproduce the two areas of good reception experimentally observed surrounding the receiver and the carrier generator (shaded regions) as described in Section 2. The discrepancies in the transition regions (around 50 cm and 250 cm) are due to the hard cutoff of the UDGMCAs model. Note that the model is nevertheless accurate within the IEEE 802.15.4 standard definition of sensitivity: The threshold signal strength above which the PRR is above 99%. This happens within 30 cm of either end in Figure 8 (shaded regions). The model could be extended in the future to more realistically simulate the transition region with a softer cutoff along with other propagation effects.

We choose $R_1 + R_2 = 300$ cm for the experiment of Figure 8 to clearly illustrate the separation between the two zones of flawless reception, given that for $R_1 + R_2 = 200$ cm as in Figure 7 these zones are merged into a continuous area of flawless reception. Conversely, performing the experiment of Figure 7 for $R_1 + R_2 = 300$ cm would cause the lowest part of the curve to lay below the noise floor of the receiver, making it impossible to measure.

We now replicate a similar experiment as the one above but for the carrier-assisted receiver. The goal is to reproduce the two areas of flawless reception of the carrier-assisted receiver as discussed in Section 2.

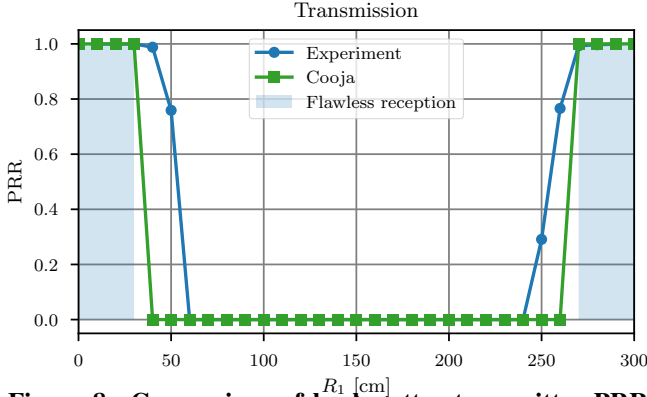


Figure 8. Comparison of backscatter transmitter PRR between experiment and simulation for $R_1 + R_2 = 300$ cm. There is a close agreement between the experimental results and the Cooja simulation. Cooja correctly simulates the two zones of flawless reception.

Setup. We place two active nodes in the same way as before ($R_1 + R_2 = 300$ cm) but this time they act as carrier generator and transmitter. The receiver requires the carrier in order to be able to receive data as discussed in Section 2. We move the carrier-assisted device like before but this time it logs the received packets in order to compute the PRR. We perform this experiment with real nodes in the anechoic chamber and in a Cooja simulation to compare the results.

Result. Figure 9 shows the result of the simulated experiment alongside the ones from the real-world experiment. Note that our model reproduces the characteristic behavior of the carrier-assisted receiver observed in experiments of having two areas of flawless reception, next to the transmitter and next to the carrier generator (shaded regions). The location and dimensions of these two areas in the simulation closely match those in the experimental results.

4.2 Simulation of Particular Effects

The previous results have shown that our model and Cooja extension reproduce the most basic properties of carrier-assisted transmissions and receptions. Real-world wireless network scenarios, however, are much more complex than the simple three-node experiments we presented before. We now examine how our Cooja extension is able to reproduce particular effects that only appear in carrier-assisted devices. As the number of nodes in the network increases, so does the probability of collisions and other similar situations. These cases are of great importance in the analysis and development of communication protocols. There is a number of new effects that have no parallel in conventional communication links. Hence, they need to be carefully considered in the development of upper-layer communication protocols. We now illustrate how our model is able to reproduce those effects accurately.

When multiple unmodulated carriers on different channels impinge on a backscatter transmitter, it will generate an equal number of reflected transmissions on the corresponding channels (two channels above each carrier, as discussed in Section 2). This effect has been demonstrated and exploited by Varshney et al. [31] to increase the robustness of backscatter transmissions. We now illustrate the same effect

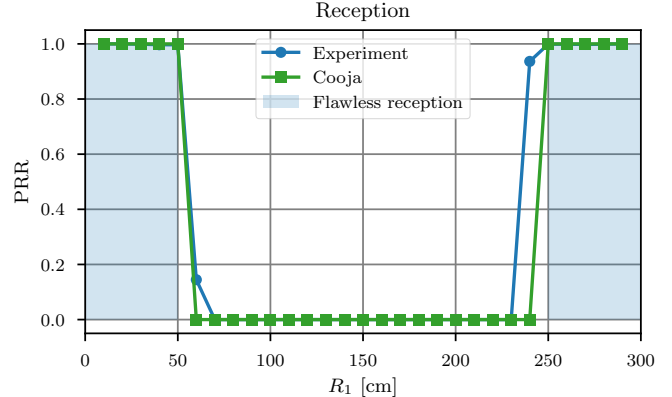


Figure 9. Comparison of carrier-assisted receiver PRR between experiment and simulation for $R_1 + R_2 = 300$ cm. There is a close agreement between the experimental results and the Cooja simulation. Cooja correctly simulates the two zones of flawless reception.

reproduced in the Cooja simulator.

Setup. We simulate a scenario (Figure 10) where three nodes act concurrently as carrier generators while three other conventional nodes act as receivers. There is a single carrier-assisted device in transmitter mode in range of all of the active nodes.

Result. Because the unmodulated carriers are sufficiently spaced in the frequency domain (four-channel spacing), the backscatter device can reflect each one of them into the corresponding channel without causing any collisions or interference at the receivers. As a result all three receivers can receive the same backscattered frame on their corresponding channels. The lower panel on Figure 10 shows the timeline as this happens. Nodes 1 to 3 generate an unmodulated carrier. Because the three carriers impinge on the carrier-assisted device (Node 4) while it transmits, three reflections are created. The three reflections reach nodes 5 to 7 that are all able to receive the backscattered transmissions at their respective channels.

The fact that backscatter devices reflect any impinging signal at no extra energy cost can be exploited for beneficial purposes as in the previous example. However, the same effect could have undesired consequences in other cases. Consider the situation depicted in Figure 11.

Setup. Figure 11 shows two conventional nodes (1 and 4) that exchange communications on channel 20 while a third node (2) located nearby transmits data on channel 18. A carrier-assisted transceiver (Node 3), located in the vicinity of Node 4, attempts to transmit at the same time.

Result. Regular communications happening two channels apart from each other would not normally pose any problem. However, the carrier-assisted device (Node 3) in the vicinity of the receiver node (4) could create a reflection of the transmission on channel 18 that is strong enough to interfere with the reception on channel 20. This happens because the backscatter device makes no distinction between reflecting an unmodulated carrier and a data-carrying signal. The reflected signal in the second case is not meaningful and cannot

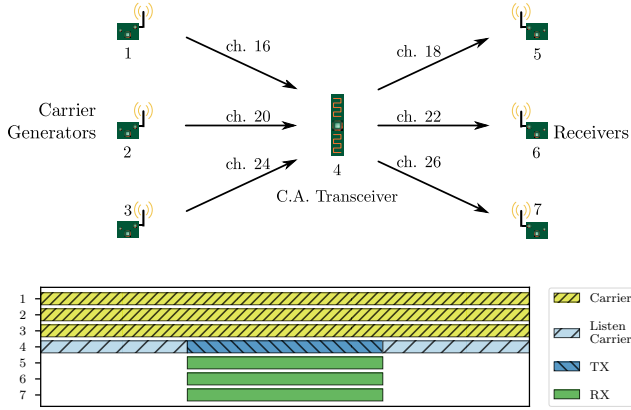


Figure 10. Multi-carrier backscatter. Multiple backscatter reflections are generated from multiple carrier generators (Nodes 1 to 3). The multiple reflections are concurrently received by receivers (Nodes 5 to 7) tuned to the corresponding channels. The timeline shows the three concurrent receptions from a single backscatter transmission.

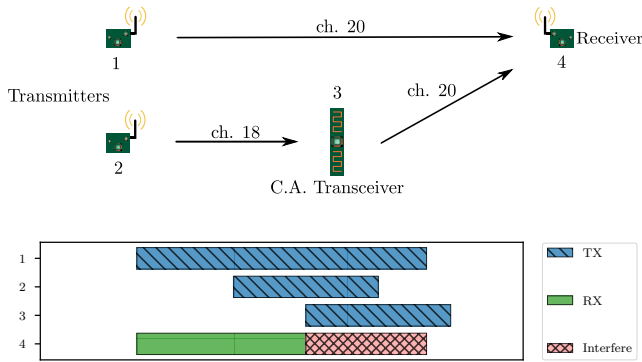


Figure 11. Unintended reflection causing interference. Backscatter transmissions can cause interference for nearby devices. The carrier-assisted device (Node 3) reflects a signal from Node 2 on channel 18 into channel 20 causing interference for the receiver (Node 4).

be received, but it has the potential to interfere with another ongoing transmission. The timeline on the lower panel of Figure 11 shows Node 1 successfully transmitting to Node 4, both conventional nodes, on channel 20. The transmissions continue undisturbed even while another conventional node (Node 2) transmits nearby on channel 18. However, when the carrier-assisted device (Node 3) attempts to transmit data and hence reflects the signal on channel 18 into channel 20, it creates interference for Node 4 and destroys the ongoing transmission to that node.

As mentioned in Section 2, the carrier-assisted receiver is vulnerable to interference from multiple unmodulated carriers in nearby frequencies. This vulnerability stems from the image frequencies of the diode mixer. We now show how this effect could have an impact in the design of future communication protocols and how our Cooja extension accurately simulates the effect.

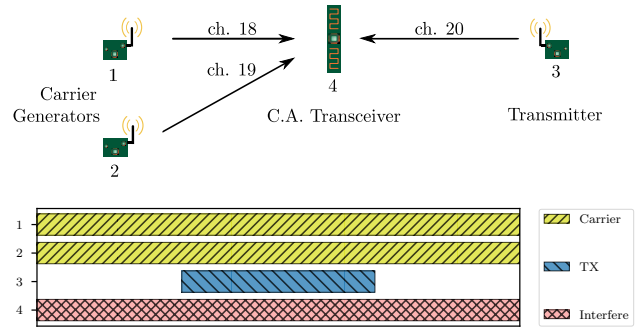


Figure 12. Carrier-assisted receiver interfered by multiple carriers. The carrier-assisted receiver (Node 4) misses a transmission from Node 3 because it is interfered by two carriers at close frequency.

Setup. Figure 12 shows two conventional 802.15.4 nodes (1 and 3) that cooperate so that the carrier-assisted transceiver (Node 4) can receive a frame on channel 20 with an unmodulated carrier on channel 18. A third conventional node (2) located in the vicinity of the carrier-assisted transceiver generates another unmodulated carrier on channel 19, possibly to support other carrier-assisted communications.

Result. The second unmodulated carrier is within the vulnerable region of the carrier-assisted receiver as discussed in Section 2. This means it is within two channels of the data transmission. As a consequence the receiver is interfered and is unable to receive the data packets. As shown in the timeline of Figure 12, our Cooja extension simulates this effect correctly. While both carriers from nodes 1 and 2 are active, the carrier-assisted device (Node 4) is considered interfered as shown on the timeline, even though the carriers are on different channels. Because the carrier-assisted device is under interference, it misses the data transmission from Node 3.

The previous results show that our model and Cooja implementation correctly simulate several important effects that are specific to carrier-assisted communications and that need to be taken into account in the development of communication protocols for carrier-assisted devices.

4.3 Evaluation of Communication Protocols

We compare the energy efficiency of three MAC protocols to illustrate how a protocol designer could employ our Cooja extension. In this proof-of-concept scenario (actual protocol development is outside the scope of this work), we focus on Pure ALOHA [1], Slotted ALOHA [26] and a TDMA-style fixed slot assignment inspired by TSCH [13].

Setup. We simulate a scenario where two conventional nodes act as carrier generator and receiver to collect data from a variable number (N) of nearby carrier-assisted devices. In this example we illustrate with a small number of carrier-assisted devices (up to four) because their short communication range limits the collision domain. Simulations with more nodes are easily realizable nonetheless. For simplicity, in this scenario the carrier generator is constantly active and the receiver node is always listening but within Cooja we can simulate arbitrarily complicated protocols with ease. We program the carrier-assisted devices to employ one

of the three MAC protocols we implemented. For each protocol we vary the number of carrier-assisted devices. During every simulated experiment the carrier-assisted devices transmit their data and the receiver logs all received packets. We employ our new Powertrace functionality on the carrier-assisted devices to compute the average energy spent per useful transmitted packet in every case. In our evaluation, we focus only on the energy consumption of carrier-assisted devices, as that is the scope of this work. Cooja already provides functionality to study the energy consumption of conventional nodes. The final result is averaged over 50 simulation runs.

For the energy computations we employ power consumption estimates for Integrated Circuit (IC) realizations of these devices as reported in the literature. We adopt a power consumption of $30 \mu\text{W}$ for the device in transmit mode based on estimates reported in several backscatter works [14, 15, 33]. For the device in receive mode, we adopt our earlier estimate of $361 \mu\text{W}$ [25]. These figures are obtained by IC power estimation methods and not from direct measurements because actual battery-free ICs are too costly to produce in small scale. For the same reason, we are unable to directly validate the Cooja-based energy estimation by comparing to experiments with a real integrated prototype. Nevertheless, we are confident in the accuracy of the results. The task of the energy estimation in Cooja is ultimately to compute the time the transceiver device spends in each of its modes (Idle, Transmit, Receive) so that the consumed energy can be computed by multiplying that time by the power consumption. We have found the computed time to be correct by comparing it to theoretical values.

Result. In ALOHA-style protocols, where frames are transmitted randomly and without collision avoidance, the probability of collisions increases with the number of transmitters, thus forcing an increase in the likelihood of retransmissions. Hence the energy per useful packet increases as we add more carrier-assisted devices, as shown in Figure 13. Our evaluation results show that the Pure ALOHA strategy, the simplest of all, scales poorly with the number of nodes. Slotted ALOHA has better performance in this regard, while TDMA performs best. The energy consumed per useful packet does not change in the TDMA protocol as there are no collisions and consequently no need for retransmissions.

The results in Figure 13 reflect the fact that time-slotted protocols, like Slotted ALOHA and TDMA, perform much better than non-slotted ones like Pure ALOHA. The time-slotted approach, however, requires nodes to be synchronized to a common clock. This creates the need for receiving synchronization beacons at the battery-free devices, which represent an additional energy investment. At this point the protocol designer would need to decide if this investment is viable. To make her decision, the designer could employ Cooja to evaluate the cost of acquiring synchronization and to fine tune parameters to reach the best possible strategy.

We devise another experiment to further illustrate how our extended Cooja could help the designer make an informed decision. We implement three different network join strategies: First, in *Periodic listening*, the carrier-assisted device periodically listens to the medium for 20 ms in every 400 ms

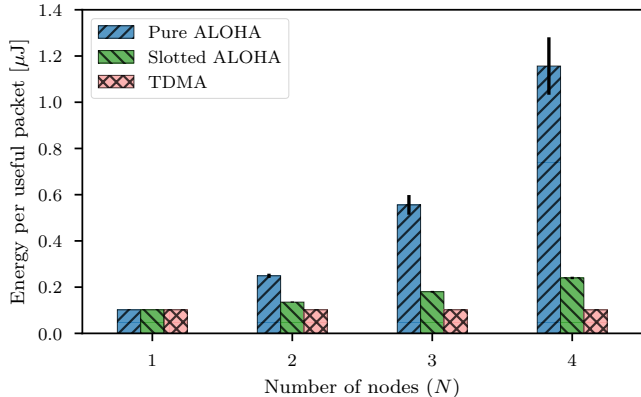


Figure 13. Comparison of energy efficiency of protocols using Cooja. We employ the extended Powertrace functionality to compute the energy per useful packet of MAC protocols. Slotted protocols perform and scale better but require time synchronization.

until it receives a beacon. When not listening, the device remains in an energy-preserving sleep state. Second, in *Constant listening*, the carrier-assisted device keeps its receiver on while constantly listening until a beacon arrives. Third, in *Active join request*, the carrier-assisted device sends a join request and immediately listens for an acknowledgement containing the necessary information.

Setup. We simulate the same scenario as before, where two conventional nodes act as carrier generator and receiver. The receiver node is always listening as before but now it also emits periodic beacons at a variable interval (τ). The carrier generator is always active too. A carrier-assisted node is turned on at a random time and attempts to join the network using the three strategies described above. For each strategy we vary the beacon interval, except for the third strategy where it is not applicable as there is no periodic beacons. During every simulated experiment we employ Powertrace at the carrier-assisted device to compute the total energy used in order to join the network. Every instance of the experiment is simulated 100 times. For the energy computations we employ the same power consumption estimates as before.

Result. Figure 14 shows the results of the experiment. The figure shows that the Periodic listening strategy consumes the most energy for joining, while the Active join request approach consumes the least.

The leftmost graph in Figure 14 shows the energy per join for the Periodic listening strategy. When the carrier-assisted device listens periodically for beacons, there is a probability that the beacon arrives during the time it sleeps. When beacons are sent more frequently, the carrier-assisted device is likely to join more quickly, consuming less energy. The graph in the middle of the figure shows the energy cost to join for the Constant listening strategy. When the carrier-assisted device is always listening it can join as soon as the beacon is received. The Active join request shows the lowest energy consumption. The time the carrier-assisted device is turned on is drastically reduced when it requests to join and receives the acknowledgement right away. This works

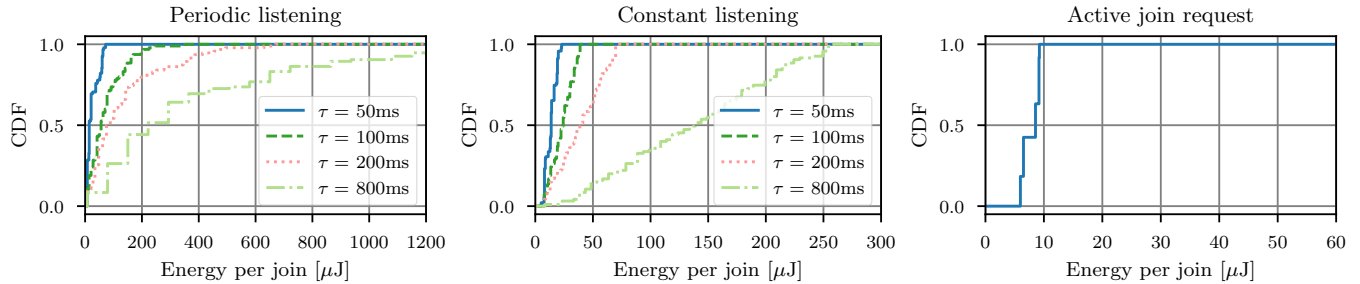


Figure 14. Comparison of the energy efficiency of network join strategies. Our Cooja extension helps easily select and tune the most energy efficient join strategy for a particular scenario. It is of note that constant listening is more efficient than periodic listening. The best approach is active join request because the clock source node is always listening.

because the receiver node is always listening in order collect all the sensor data from the previous example.

These simplified scenarios show our Cooja extension helps easily compare and tune parameters in communication protocols bringing valuable insights for the development of carrier-assisted protocols.

5 Related Work

The Cooja simulator [21] has been designed to develop sensor network software and applications, and to profile their energy consumption [9]. We extend Cooja with carrier-assisted communications, which enables the simulation of heterogeneous networks of battery-free sensor nodes and conventional ones. Existing simulators such as Castalia [5] and TOSSIM [17, 28] do not provide such facilities.

Other works use frameworks like Omnet++ and ns-3 to simulate passive RFID communications [10, 19, 35]. RFID systems employ backscatter for transmissions but are limited by the need for a complicated and expensive reader, and are not compatible with commodity protocols such as IEEE 802.15.4, commonly employed in sensor network applications. As a consequence, they cannot seamlessly integrate with existing networks. Our work focuses on the simulation of standard-compatible carrier-assisted communications. While we also employ backscatter communications for transmissions, we go one step further with frequency-shifted backscatter of 802.15.4 and carrier-assisted receivers enabling the seamless integration of these devices with existing networks.

GreenCastalia [3] is a framework for the Castalia simulator to support energy-harvesting systems. GreenCastalia provides support for, e.g., multiple energy sources, multi-source harvesters as well as supercapacitors and rechargeable batteries. In a similar effort, Tapparello et al. [29] have extended the energy framework of ns-3 to include energy harvesting capabilities. These efforts are orthogonal to our work since we focus on including novel ultra-low power communication mechanisms in the Cooja simulator. These mechanisms drastically decrease energy consumption which reduces the amount of energy nodes need to harvest.

Ekho [12] is a hardware emulator designed to record energy harvesting conditions enabling to recreate those conditions in the lab. Related tools such as SunaPlayer [4] and LightBox [27] focus on specific harvesting modalities, namely solar energy. Enspect [30] not only provides data

collection but also analysis software to model the performance of energy harvesting systems.

In order to simulate intermittently powered devices, Furlong et al. [11] have developed SIREN. SIREN extends MSPSim [8], an instruction level simulator for sensor boards with peripherals that is incorporated in Cooja’s cross-level simulation environment. SIREN uses Ekho’s energy recording capabilities and provides support for the creation of artificial (estimated or random) energy environments. In addition, it extends MSPSim with new peripherals such as FRAM. Again, our work is orthogonal in that it allows the simulation of carrier-assisted communications which enables battery-free devices by drastically reducing the energy required for communication. At the same time, our work is complementary to SIREN in that we focus on carrier-assisted communications while SIREN handles aspects related to harvesting and energy management in the same Cooja framework.

6 Conclusions

We introduced models to simulate carrier-assisted communications between battery-free devices and unmodified conventional radios. To the best of our knowledge our Cooja extension is the first network simulator that supports standard-compatible carrier-assisted communications.

Our model accurately reproduces the basic characteristics of carrier-assisted communications in terms of range and vulnerability to interference, both for reception and transmission. As a result, Cooja can now accurately reproduce several important effects such as frequency-shifted interference, that are specific to carrier assisted communications. Our extended Cooja maintains compatibility with all the energy estimation tools already available in Cooja, making it a valuable tool to evaluate and compare the energy efficiency of protocols. We believe all this makes the extended Cooja a valuable tool for the community to experiment with these devices despite the lack of access to real-world prototypes and can help develop future communication protocols for them. The extended Cooja is available from: <https://github.com/cperezpenichet/contiki-ng/tree/carrier-assisted>

7 Acknowledgments

We thank Ambuj Varshney for his initial ideas towards this work. This work has been partly funded by the Swedish Research Council (Grant 2017-045989).

8 References

- [1] N. Abramson. The ALOHA System: Another alternative for computer communications. In *Proceedings of the November 17-19, 1970, fall joint computer conference*. ACM, 1970.
- [2] C. A. Balanis. *Antenna Theory: Analysis and Design*. Wiley-Interscience, 3rd edition, 2005.
- [3] D. Benedetti, C. Petrioli, and D. Spenza. GreenCastalia: An Energy-harvesting-enabled Framework for the Castalia Simulator. In *Proceedings of the 1st International Workshop on Energy Neutral Sensing Systems*, ENSSys '13. ACM, 2013.
- [4] S. Bobovych, N. Banerjee, R. Robucci, J. P. Parkerson, J. Schmandt, and C. Patel. Sunaplayer: high-accuracy emulation of solar cells. In *Proceedings of the 14th International Conference on Information Processing in Sensor Networks*, IPSN '15. ACM, 2015.
- [5] A. Boulis. Castalia: Revealing Pitfalls in Designing Distributed Algorithms in WSN. In *Proceedings of the 5th International Conference on Embedded Networked Sensor Systems*, SenSys '07. ACM, 2007.
- [6] J. F. Ensworth, A. T. Hoang, and M. S. Reynolds. A low power 2.4 GHz superheterodyne receiver architecture with external LO for wirelessly powered backscatter tags and sensors. In *2017 IEEE International Conference on RFID*, IEEE RFID, 2017.
- [7] J. F. Ensworth and M. S. Reynolds. Every smart phone is a backscatter reader: Modulated backscatter compatibility with Bluetooth 4.0 Low Energy (BLE) devices. IEEE RFID, 2015.
- [8] J. Eriksson, A. Dunkels, N. Finne, F. Österlind, and T. Voigt. MSPsim – an extensible simulator for MSP430-equipped sensor boards. Proceedings of the European Conference on Wireless Sensor Networks (EWSN), 2007.
- [9] J. Eriksson, F. Österlind, N. Finne, N. Tsiftes, A. Dunkels, and T. Voigt. Accurate Network-Scale Power Profiling for Sensor Network Simulators. Proceedings of the European Conference on Wireless Sensor Networks (EWSN), 2009.
- [10] C. Floerkemeier and S. Sarma. RFIDSim—a physical and logical layer simulation engine for passive RFID. *IEEE Transactions on Automation Science and Engineering*, 2009.
- [11] M. Furlong, J. Hester, K. Storer, and J. Sorber. Realistic simulation for tiny batteryless sensors. In *Proceedings of the 4th International Workshop on Energy Harvesting and Energy-Neutral Sensing Systems*. ACM, 2016.
- [12] J. Hester, T. Scott, and J. Sorber. Ekho: Realistic and Repeatable Experimentation for Tiny Energy-harvesting Sensors. In *Proceedings of the 12th ACM Conference on Embedded Network Sensor Systems*, SenSys '14. ACM, 2014.
- [13] IEEE. *IEEE 802.15.4 Standard for Low-Rate Wireless Networks*. 2015.
- [14] V. Iyer, V. Talla, B. Kellogg, S. Gollakota, and J. Smith. Inter-Technology Backscatter: Towards Internet Connectivity for Implanted Devices. In *Proceedings of the 2016 ACM SIGCOMM Conference*. ACM, 2016.
- [15] B. Kellogg, V. Talla, S. Gollakota, and J. R. Smith. Passive Wi-Fi: Bringing Low Power to Wi-Fi Transmissions. NSDI '16, 2016.
- [16] J. Ko, J. Eriksson, N. Tsiftes, S. Dawson-Haggerty, J.-P. Vasseur, M. Durvy, A. Terzis, A. Dunkels, and D. Culler. Beyond Interoperability: Pushing the Performance of Sensor Network IP Stacks. In *Proceedings of the 9th ACM Conference on Embedded Networked Sensor Systems*, SenSys '11. ACM, 2011.
- [17] P. Levis, N. Lee, M. Welsh, and D. Culler. TOSSIM: accurate and scalable simulation of entire tinyOS applications. In *Proceedings of the International Conference on Embedded Networked Sensor Systems (ACM SenSys)*, 2003.
- [18] V. Liu, A. Parks, V. Talla, S. Gollakota, D. Wetherall, and J. R. Smith. Ambient Backscatter: Wireless Communication out of Thin Air. In *Proceedings of the ACM SIGCOMM 2013 Conference*. ACM, 2013.
- [19] I. Mayordomo, R. Berenguer, I. Fernandez, I. Gutierrez, W. Strauss, and J. Bernhard. Simulation and measurement of a long-range passive RFID system focused on reader architecture and backscattering communication. In *38th European Microwave Conference*, 2008.
- [20] R. Nandakumar, V. Iyer, and S. Gollakota. 3D Localization for Sub-Centimeter Sized Devices. In *Proceedings of the 16th ACM Conference on Embedded Networked Sensor Systems*, SenSys. ACM, 2018.
- [21] F. Österlind, A. Dunkels, J. Eriksson, N. Finne, and T. Voigt. Cross-level sensor network simulation with cooja. In *Proceedings of the First IEEE International Workshop on Practical Issues in Building Sensor Network Applications (SenseApp 2006)*, 2006.
- [22] P. Pannuto, B. Kempke, and P. Dutta. Slocalization: sub- μ W ultra wideband backscatter localization. In *Proceedings of the 17th ACM/IEEE International Conference on Information Processing in Sensor Networks*, IPSN '18. IEEE Press, 2018.
- [23] D. Pozar. *Microwave Engineering*. Wiley, 4th edition, 2011.
- [24] C. Pérez-Penichet, F. Hermans, A. Varshney, and T. Voigt. Augmenting IoT Networks with Backscatter-enabled Passive Sensor Tags. In *Proceedings of the 3rd Workshop on Hot Topics in Wireless*, HotWireless '16. ACM, 2016.
- [25] C. Pérez-Penichet, C. Noda, A. Varshney, and T. Voigt. Battery-free 802.15.4 Receiver. In *Proceedings of the 17th ACM/IEEE International Conference on Information Processing in Sensor Networks*, IPSN '18. IEEE Press, 2018.
- [26] L. G. Roberts. ALOHA Packet System with and Without Slots and Capture. *SIGCOMM Comput. Commun. Rev.*, (2), 1975.
- [27] J. Sarik, K. Kim, M. Gorlatova, I. Kymissis, and G. Zussman. More than meets the eye—a portable measurement unit for characterizing light energy availability. In *Global Conference on Signal and Information Processing (GlobalSIP)*. IEEE, 2013.
- [28] V. Shnayder, M. Hempstead, B. Chen, and M. Welsh. PowerTOSSIM: Efficient power simulation for tinyos applications. In *Proceedings of the International Conference on Embedded Networked Sensor Systems (ACM SenSys)*, 2004.
- [29] C. Tapparello, H. Ayatollahi, and W. Heinzelman. Energy harvesting framework for network simulator 3 (ns-3). In *Proceedings of the 2nd International Workshop on Energy Neutral Sensing Systems*. ACM, 2014.
- [30] N. F. Tinsley, S. T. Witts, J. M. Ansell, E. Barnes, S. M. Jenkins, D. Raveendran, G. V. Merrett, and A. S. Weddell. Enspect: A Complete Tool Using Modeling and Real Data to Assist the Design of Energy Harvesting Systems. In *Proceedings of the 3rd International Workshop on Energy Harvesting & Energy Neutral Sensing Systems*, ENSSys '15. ACM, 2015.
- [31] A. Varshney, O. Harms, C. Pérez-Penichet, C. Rohner, F. Hermans, and T. Voigt. LoRea: A Backscatter architecture that achieves a long communication range. In *SenSys 2017*. ACM, 2017.
- [32] A. Wang, V. Iyer, V. Talla, J. R. Smith, and S. Gollakota. FM Backscatter: Enabling Connected Cities and Smart Fabrics. In *NSDI '17*, 2017.
- [33] P. Zhang, D. Bharadia, K. Joshi, and S. Katti. HitchHike: Practical Backscatter Using Commodity WiFi. In *Proceedings of the 14th ACM Conference on Embedded Network Sensor Systems*, SenSys '16. ACM, 2016.
- [34] P. Zhang, M. Rostami, P. Hu, and D. Ganesan. Enabling Practical Backscatter Communication for On-body Sensors. In *Proceedings of the 2016 SIGCOMM Conference*, SIGCOMM '16. ACM, 2016.
- [35] L. Zhou, F. Hutu, G. Villemaud, and Y. Duroc. Simulation framework for performance evaluation of passive RFID tag-to-tag communications. In *2017 11th European Conference on Antennas and Propagation (EUCAP)*, 2017.